Degradation Status Recognition of Axial Piston Pumps under Variable Conditions Based on Improved Information Entropy and Gaussian Mixture Models

Chuanqi Lu [1], **Zhi Zheng [2]** and **Shaoping Wang [3],***

[1] College of Engineering, Huazhong Agricultural University, Wuhan 430070, China; luchuanqi1987@buaa.edu.cn

[2] College of Mechanical Engineering, North China University of Science and Technology, Tangshan 063210, China; zhengzhi@ncst.edu.cn

[3] School of Automation Science and Electrical Engineering, Beihang University, Beijing 100191, China

* Correspondence: shaopingwang@buaa.edu.cn

Abstract: Axial piston pumps are crucial for the safe operation of hydraulic systems and usually work under variable operating conditions. However, deterioration status recognition for such pumps under variable conditions has rarely been reported until now. Therefore, it is valuable to develop effective methods suitable for processing variable conditions. Firstly, considering that information entropy has strong robustness to variable conditions and empirical mode decomposition (EMD) has the advantages of processing nonlinear and nonstationary signals, a new degradation feature parameter, named local instantaneous energy moment entropy, which combines information entropy theory and EMD, is proposed in this paper. To obtain more accurate degradation feature, a waveform matching extrema mirror extension EMD, which is used to suppress the end effects of EMD decomposition, was employed to decompose the original pump's outlet pressure signals, taking the quasi-periodic characteristics of the signals into consideration. Subsequently, given that different failure modes of pumps have different degradation rates in practice, which makes it difficult to effectively recognize degradation status when using the modeling methods that need the normal and failure data, a Gaussian mixture model (GMM), which has no need for failure data when building a degradation identification model, was introduced to capture the new degradation status index (DSI) to quantitatively assess the degradation state of the pumps. Finally, the effectiveness of the proposed approach was validated using both simulations and experiments. It was demonstrated that the defined local instantaneous energy moment entropy is able to effectively characterize the degree of degradation of the pumps under variable operating conditions, and the DSI derived from the GMM is able to accurately identify different degradation states when compared with the previously published methods.

Keywords: degradation identification; energy moment entropy; waveform matching extrema mirror extension EMD; Gaussian mixture model; axial piston pump

1. Introduction

Hydraulic systems are some of the most important subsystems that are used in various industrial applications, such as aircraft, hoisting machinery, and roller mills [1]. Axial piston pumps are the core component of hydraulic systems and they supply pressurized oil to the hydraulic actuators. Once a pump fails, it will result in the function degradation of the hydraulic system and can even cause the unplanned breakdown of the machines they are part of [2,3]; hence, failure of the pumps should be diagnosed as early as possible. However, in the same way as most mechanical components, axial

piston pumps will experience different states of degradation: From a healthy state to its final failure state. This means that fault diagnosis would be more meaningful if the states of degradation could be reliably identified. In other words, developing an efficient degradation status identification method for axial piston pumps is vital if unexpected failure is to be prevented.

In recent decades, condition-based maintenance has become a vital technology that is used to improve the safety and reliability of pumps. Therefore, increasing attention has been paid to recognizing the degradation states of pumps, as this is the fundamental element of condition-based maintenance [4–6]. Although some methods have been successfully applied to identify the degradation states of pumps, most of the studies assumed that the pumps operated at a constant condition when carrying out identification of the degradation states; in real-world applications, this may not be the case due to different load spectra. So far, less study has been done on the research of degradation status recognition of the pump under variable operating conditions. Apart from this, most of the methods were based on vibration signal or return oil flow signal, but a large number of studies have shown that the pump's discharge pressure possesses a rich variety of state information [7–10]. Hence, this paper concentrated on developing a method to recognize the deterioration status, based on the pump's outlet pressure signal, which is suitable for variable operating conditions.

One of the main challenges of developing the method is how to extract the sensitive features that track the trend of the degradation status of a pump under variable operating conditions. Previous studies have indicated that dimensionless indices can be used to monitor the condition of the equipment under variable conditions as they are theoretically not affected by the operational status of the equipment [11,12]. Traditional dimensionless indices, such as the waveform index, the crest index, the kurtosis index, etc., are sensitive to identify the failure modes of a pump under variable conditions. However, they cannot effectively characterize the severity of a fault in a pump as they are not sufficiently stable [5]. Considering that information entropy, which is a dimensionless parameter, can describe the complexity of a time series, many information entropies, such as power spectrum entropy (PSE) [13], singular spectrum entropy (SSE) [14], sample entropy (SE) [15], etc., have been used as a degradation feature to recognize the severity of a fault in rotating machines [16–18]. Although these information entropies have shown remarkable performance, it is difficult to obtain satisfactory results in some cases. For example, pump outlet pressure signals have obvious nonstationary characteristics, but power spectrum analysis is a global transform that is suitable for processing stationary signals. Meanwhile, some information entropies are calculated in the original time-domain space, which means that the calculation results are easily disturbed by the noise. To solve these problems, some researchers combined time-frequency analysis methods with information entropy theory [19–22]. Among these methods, empirical mode decomposition (EMD) has no need for presetting parameters compared with wavelet analysis (WT) and variational mode decomposition (VMD). Thus, the feature extraction method, which combines EMD with information entropy theory, has been used to identify the severity of a fault in a pump [19], but some drawbacks still exist. For instance, this method does not consider the influence of end effects, which seriously affect the decomposition accuracy of EMD; furthermore, the accuracy of the information entropy will also be affected. At present, many methods have been proposed to suppress the end effects resulting from EMD [23–29]. Among these methods, the extrema mirror extension-based EMD that was proposed by Rilling [29] has been most widely used due to its outstanding performance. Nevertheless, it is difficult to obtain satisfactory results if the endpoints are not extrema when directly performing Rilling's extrema mirror extension-based EMD [28]. Given that the discharge pressure signal of the piston pump is a quasi-periodic signal, Lu et al. [30] combined waveform matching and extrema mirror extension-based EMD to restrain the end effects and the experimental analysis demonstrated that the improved EMD could capture the intrinsic mode functions (IMFs) with high accuracy. Hence, the improved EMD was introduced to obtain more accurate information entropy in this paper.

Another challenge in this paper was the construction of an effective intelligent model to assess the state of a pump. To date, machine learning technologies, such as support vector machines (SVM) [31],

support vector data description (SVDD) [32], support vector regression (SVR) [33], neural networks (NN) [34–36], fuzzy c-means clustering (FCM) [37–39], etc., have been widely used to solve the modeling problem when performing degradation status recognition in other rotating machines. Although the effectiveness of these methods has been indicated, it is still difficult to obtain satisfactory results in some cases. For instance, most of these methods adopt samples from various degradation states for their training. However, an axial piston pump, as a highly integrated mechatronics component, has many failure modes. This means that its degradation states are not identical due to the different failure degradation rates, which will make it difficult to obtain complete degradation states' training samples. Although some methods including self-organization mapping (SOM) network, SVDD, etc. only utilize the normal data to model, the key parameters of these methods need to be set in advance based on experiences that affect the adaptability of the methods. Therefore, these modeling methods can hardly be directly applied to identify the deterioration status of an axial piston pump. As previous research has shown, the distribution of the feature vectors that are extracted from a pump's pressure signals is a stochastic process in the feature space; therefore, probability models can be used to describe the distribution. Among the various probability models is the Gaussian mixture model (GMM). This has the advantage of approximating the arbitrary probability density function through the use of several Gaussian probability distribution functions (PDF). Moreover, only normal state data are used to build the model when performing degradation status recognition. Consequently, the GMM was introduced to identify the deterioration states of axial piston pumps in this work.

The main contributions of this paper are as follows. On the one hand, a new dimensionless parameter, namely the local instantaneous energy moment entropy that is obtained from the waveform matching extrema mirror extension EMD, is defined as the degradation feature of the pump under variable conditions. On the other hand, a new degradation status index (DSI), which is derived from GMM, was proposed to identify the pump's deterioration status adaptively.

The remainder of this paper is organized as follows. Section 2 presents the degradation status identification method that is based on the improved information entropy and the GMM. In Section 3, the proposed method is validated by both simulations and experiments. Finally, the conclusions are given in Section 4.

2. Degradation Status Identification Method

2.1. Degradation Feature Extraction

As previously noted, the information entropies, which have strong robustness to variable conditions, have been successfully applied in the fault diagnosis of rotating machines under variable operating conditions [5]. Nevertheless, it is difficult to achieve good performance when traditional information entropies are used in degradation status recognition of the pump. This is because some of the information entropies are only suitable for processing stationary signals, and some are not stable as they are calculated in the original time-domain space. Consequently, a new information entropy needs to be developed. Considering that EMD is one of the most powerful time-frequency analysis methods, the feature extraction method which combines EMD and information entropy theory is proposed in this section.

2.1.1. Waveform Matching Extrema Mirror Extension EMD

Although EMD shows excellent performance in feature extraction when performing fault diagnosis of the pump, some drawbacks still exist, one of which is end effects. Previous studies have shown that end effects will decrease the accuracy of the IMFs seriously. In other words, end effects needs to be restrained to obtain more accurate IMFs. Currently, many useful methods have been developed to suppress the end effects; among these methods, it is proved that the extrema mirror extension EMD can significantly suppress the end effects when processing integer periodic signals [30]. This means

that high-precision IMFs can be acquired if the decomposed pump's discharge pressure signals take the form of full periodic signals.

Theoretically, the discharge pressure signal of an axial piston pump is a standard sinusoidal signal; however, the actual pressure signal will become a quasi-periodic signal, particularly when certain faults occur. Therefore, it is difficult for the traditional full-cycle sampling methods to directly process the pump's outlet pressure signal. Fortunately, this limitation can be solved by the extension methods as they consider the characteristics of the pump's discharge pressure signal. Based on these analyses, an improved EMD algorithm that combines waveform matching with extrema mirror extension was utilized in this section. The proposed method mainly involves three key steps: Namely, full-cycle signal extension based on waveform matching, signal decomposition using extrema mirror extension EMD, and signal interception based on the position and length of the original time series. Following this, the proposed algorithm was covered in detail.

In the signal acquisition process, the collected signals are not usually full-cycle signals due to the randomness of signal interception and the difficulty of achieving accurate full-cycle sampling. In order to improve its generality, it was supposed that $Y(t)$ is a non-integer periodic discrete signal, defined as follows:

$$Y(t) = [y_1, y_2, \ldots, y_n], \quad t = [t_1, t_2, \ldots, t_n], \quad t \neq mT, \quad m \in N_+ \tag{1}$$

where n is the length of the signal series and T is the period of the signal.

According to the above analysis, the original signal, $Y(t)$, needs to be extended via the waveform matching method. The key part of the waveform matching extension is to discover the matching waveform with the highest similarity to the target waveform near its end points. To find the most suitable matching wave, a reasonable waveform matching index must first be defined. Although numerous methods have been used to calculate the similarity between two time series, some methods have mainly focused on the difference in the distance while others have paid attention to the difference in the direction. In order to simultaneously consider the differences in both the distance and direction, a waveform matching index can be written as follows:

$$\sigma = \frac{x_1(t) \cdot x_2(t)}{\|x_1(t)\|^2 + \|x_2(t)\|^2 - x_1(t) \cdot x_2(t)} \tag{2}$$

where $x_1(t)$ and $x_2(t)$ are two data sequence vectors with the same dimensions. It can be easily proven that the range of σ is between 0 and 1; in particular, the waveform matching index is 1 if and only if the two vectors are equal. Following the definition of the waveform matching index, the detailed extension process has been given below:

(1) The signal sequence $Y(t)$ was differentiated and the local minima and maxima were obtained. Then, the definitions could be given as follows:

$$\begin{cases} T_{\max}(i) = t_{I_{\max}(i)} & T_{\min}(j) = t_{I_{\min}(j)} & i = 1, 2, \ldots, M \\ U(i) = y_{I_{\max}(i)} & V(j) = y_{I_{\min}(j)} & j = 1, 2, \ldots, N \end{cases} \tag{3}$$

where $T_{\max}$ and $T_{\min}$ are the times of the local maxima and minima points, $I_{\max}$ and $I_{\min}$ are the subscripts of the local maxima and minima points in the original sequence, U and V are the function values corresponding to the local maxima and minima points, and M and N are the number of local maxima and minima points.

(2) The left extension for the signal $Y(t)$ was then executed. If the minima points of the signal appeared first, namely $I_{\min}(1) < I_{\max}(1)$, the target wave could be described as:

$$y_1(t) = [y_1, \ldots, y_{I_{\min}(1)}] \tag{4}$$

Based on Equation (4), the matching wave was then defined as:

$$y_2(t) = [y_{I_{\min}(p)-I_{\min}(1)+1}, \ldots, y_{I_{\min}(p)}] \quad p \in N_+, p > 1 \tag{5}$$

From Equation (5), it can be found that the key to solving $y_2(t)$ was to capture $I_{\min}(p)$. In order to acquire $I_{\min}(p)$, the error function was first defined as:

$$\Delta_{kj} = \quad |I_{\min}(j) - I_{\min}(1) - k \cdot T \cdot f_s| \\ k = 1, 2, \ldots, K \tag{6}$$

where f_s is the sampling frequency and K is the number of cycles. According to Equation (6), the number for Δ_{1j} is N when $k = 1$. Supposing that Δ_{1j} is the minimum while $j = p_1$, then $I_{\min}(p_1)$ could be acquired. In the same manner, $I_{\min}(p_2), \ldots, I_{\min}(p_K)$ could then be obtained.

(3) The waveform matching index r between $y_1(t)$ and $y_2(t)$ was then calculated via Equation (2). Then, the most suitable matching wave was chosen, based on the largest computed value of σ. Currently, if it can be assumed that $p = p_K$, then the left characteristic wave can be expressed as follows:

$$C_L = [y_{I_{\min}(p_{K-1})}, \ldots, y_{I_{\min}(p_K)}] \quad I_{\min}(p_0) = 1 \tag{7}$$

Accordingly, based upon Equations (3) and (7), the left extension signal $y_l(t)$ can be defined as follows:

$$y_l(t) = C_L, \quad t_l < \frac{T}{4} \\ y_l(t) = [y_{I_{\min}(p_{K-1})}, \ldots, y_{I_{\min}(p_K)-I_{\min}(1)}], \quad t_l \geq \frac{T}{4} \tag{8}$$

where t_l is the length of the left target wave $y_1(t)$. In the same way, if the maxima points of the signal appeared first, namely $I_{\max}(1) < I_{\min}(1)$, then the left characteristic wave could be expressed as follows:

$$C_L^* = [y_{I_{\max}(q_{K-1})}, \ldots, y_{I_{\max}(q_K)}] \tag{9}$$

As a result, the left extension signal $y_l(t)$ could be formulated as follows:

$$y_l(t) = C_L^*, \quad t_l < \frac{T}{4} \\ y_l(t) = [y_{I_{\max}(q_{K-1})}, \ldots, y_{I_{\max}(q_K)-I_{\max}(1)}], \quad t_l \geq \frac{T}{4} \tag{10}$$

(4) The right extension for the signal $Y(t)$ was then conducted. Firstly, the target wave was defined as follows:

$$y_1^*(t) = [y_{I_{\min}(p_K)}, \ldots, y_n], \quad I_{\max}(q_K) < I_{\min}(p_K) \\ y_1^*(t) = [y_{I_{\max}(q_K)}, \ldots, y_n], \quad I_{\max}(q_K) > I_{\min}(p_K) \tag{11}$$

By repeating steps (2) and (3), the right extension signal $y_r(t)$ could be captured.

(5) The final extended signal was then acquired $Y^*(t) = [y_l(t), \ldots, y_r(t)]$.

After the full-cycle extension of the signal was finished, the extrema mirror extension EMD was introduced to decompose the extension signal. Based on the definition of EMD, the extension signal could then be written as follows:

$$Y^*(t) = \sum_{i'=1}^{m} c_{i'}^*(t) + a(t) \tag{12}$$

where $c_{i'}^*(t)$ is the i'th IMF, m is the number of the IMFs, and $a(t)$ represents the residual component. Finally, the IMFs of the original signal $Y(t)$ could be intercepted from $c_{i'}^*(t)$ by combining the length of the original signal with its position in the extension signal.

2.1.2. Local Instantaneous Energy Moment Entropy

In the previous section, high-precision IMFs were acquired based on the proposed EMD method. As described in previous studies [19,30], the IMFs obtained from the EMD have different characteristic scales, and the characteristic scales of the IMFs that are obtained from the decomposition of the pump's pressure signals also change when the health status of the pump changes. Therefore, the key challenge in extracting the sensitive degradation features of the pump is how to effectively utilize these obtained IMFs.

As is well known, the Hilbert spectrum [29], which is constructed by applying the Hilbert transform to the obtained IMFs, is able to effectively describe the time-frequency distribution of the signal. Hence, the Hilbert spectrum-based method has been successfully used for feature extraction of the discharge pressure signals of pumps [10,19]. However, some insufficiencies still exist in these methods, one of which is that the high levels of noise in the pump's pressure signals will severely affect the results of the feature extraction. In addition, these methods do not consider the variable conditions of the pumps. Given that the local Hilbert energy spectrum is able to effectively suppress the influence of the noise and information entropy is applicable in complex working conditions, as a result, a new information entropy, namely local instantaneous energy moment entropy, which is based on the local Hilbert energy spectrum, is proposed in this section. Next, the definition process is given.

Supposing that $c_{i'}(t)$ is the i'th IMF of the original signal $Y(t)$ and $H(\omega, t)$ is the Hilbert spectrum, since the energy of the signal is conserved during the transform process, the following can be obtained:

$$\int_{-\infty}^{\infty} \left| \sum_{i'=1}^{m} c_{i'}(t) \right|^2 dt = \int_{-\infty}^{\infty} \int_{-\infty}^{\infty} H^2(\omega, t) d\omega dt \tag{13}$$

In Equation (13), the residual component is left out. From Equation (13), the instantaneous energy can be then be expressed as:

$$E(t) = \int_{-\infty}^{\infty} H^2(\omega, t) d\omega \tag{14}$$

Although the instantaneous energy is able to describe the time distribution of the signal energy, it is not sufficiently precise in some cases. Previous studies have shown that the energy moment can more accurately describe the essential characteristics of the signal [40]. Thus, the instantaneous energy moment was constructed in this paper and was defined as follows:

$$T = \sum_{z=1}^{n} (z \cdot \Delta t) |E(z \cdot \Delta t)|^2 \tag{15}$$

where z is the sampling point and Δt is the sampling interval time.

Based on the previous research [19], a different IMF has a different sensitivity to degradation feature extraction. Hence, more sensitive IMFs can be selected by calculating the correlation between each IMF and the original signal. According to the literature [41], the threshold is usually set to 0.2. After the useful IMFs have been obtained, the local instantaneous energy moment can be written as:

$$T_k = \sum_{z=1}^{n} (z \cdot \Delta t) |E_k(z \cdot \Delta t)|^2 \tag{16}$$

where E_k denotes the instantaneous energy of the kth IMF. At this time, the feature vector can be expressed as follows:

$$\mathbf{T} = \begin{bmatrix} T_1/T' & T_2/T' & \dots & T_h/T' \end{bmatrix}$$
$$T' = \sum_{k=1}^{h} T_k \tag{17}$$

where h is the number of selected IMFs.

According to Equation (17), the local instantaneous energy moment entropy can be defined as follows:

$$H = -\sum_{r=1}^{h} \mathbf{T}(1,r)\ln(\mathbf{T}(1,r)) \tag{18}$$

2.2. Degradation Status Recognition Based on the GMM

After carrying out the degradation features' extraction of a pump, a recognition method needs to be developed to accurately identify the pump's deterioration states with the extracted features. Traditional identification methods usually need feature samples obtained from different degradation data to train the recognition model. However, there are many failure modes and these faults have different degradation rates in axial piston pumps; this makes it difficult to establish a standard sample degradation status database. GMM is different from the above methods, as it only needs the health state data to be able to construct a degradation recognition model [1]. Accordingly, the GMM has been adopted in this section to recognize the degradation status of a pump.

2.2.1. A Brief Description of the GMM

The GMM was developed to solve the problem where it is difficult for a single Gaussian PDF to accurately describe the distribution of non-ellipsoidal data. As the GMM is composed of different single Gaussian models, it can theoretically approximate any data distribution if the appropriate number of single Gaussian models is selected. If it is supposed that $Z = \{\mathbf{Z}_1, \mathbf{Z}_2, \ldots, \mathbf{Z}_{n'}\}$ is an r-dimensional dataset, then it can be described by a GMM as follows:

$$P(\mathbf{Z}) = \sum_{s=1}^{S} w_s P_s(\mathbf{Z}) = \sum_{s=1}^{S} w_s N(\mathbf{Z}, \boldsymbol{\mu}_s, \Sigma_s) \tag{19}$$

$$N(\mathbf{Z}, \boldsymbol{\mu}_s, \Sigma_s) = \frac{1}{\sqrt{(2\pi)^r |\Sigma_s|}} \exp(-\frac{1}{2}(\mathbf{Z} - \boldsymbol{\mu}_s)^T \Sigma_s^{-1}(\mathbf{Z} - \boldsymbol{\mu}_s)) \tag{20}$$

where S is the number of Gaussian models involved in the mixing, w_s is the weight of each Gaussian model and satisfies the condition where the sum of the weights is 1, $P_s(Z)$ is the PDF of the sth Gaussian model, and $\boldsymbol{\mu}_s$ and Σ_s represent the mean vector and the covariance matrix of the sth Gaussian model, respectively.

From Equation (19), it can be found that the performance of the GMM is closely related to the three key parameters. In general, the maximum likelihood estimation method can be utilized to obtain these parameters. Nevertheless, the process of solving the likelihood function of the GMM is extremely complicated and it is difficult to obtain a closed solution. The expectation maximum (EM) algorithm has been commonly used to solve this problem. The EM method mainly includes two steps, namely the E-step and the M-step; the detailed algorithm can be found in the literature [42]. Once the three parameters have been determined via the EM algorithm, the GMM can be established.

2.2.2. Degradation Status Index Obtained from the GMM

In order to quantitatively describe the degradation status of an axial piston pump, a new degradation status index (DSI), which was derived from the GMM, was defined in this section. Next, the definition process is analyzed.

The pump's outlet pressure signals if its health state were collected and then the feature vectors were extracted from the pump's healthy state pressure signals as training samples used to establish the GMM. It was supposed that $\mathbf{Z}' = \{\mathbf{Z}'_1, \mathbf{Z}'_2, \ldots, \mathbf{Z}'_O\}$ are a series of test samples that were extracted from the pump's pressure signals; the probability $P(\mathbf{Z}'_a), a = 1, 2, \ldots, O$ represented the probability of the sample $\mathbf{Z}'_a$ being generated by the GMM that was constructed using samples of a pump in its healthy

state. If the tested samples were generated from signals of the pump's degradation state, the value of $P(\mathbf{Z}'_a)$ should be less than the output value of the healthy state samples in this GMM. In other words, the value of $P(\mathbf{Z}'_a)$ should be below a certain threshold. Thus, this probability can characterize the extent to which the tested data has deviated from the healthy condition. According to the above analysis, a new DSI was then defined as follows:

$$DSI = \begin{cases} \frac{\ln(P(\mathbf{Z}'_a)+\zeta)}{\ln \zeta} & P(\mathbf{Z}'_a) + \zeta < 1 \quad \zeta \in (0,1) \\ 0 & P(\mathbf{Z}'_a) + \zeta \geq 1 \end{cases} \tag{21}$$

where ζ is a minimal positive constant. From Equation (21), it can be seen that the values of the DSI were between 0 and 1. Moreover, the values of the DSI gradually increased as $P(\mathbf{Z}'_a)$ decreased; in particular, the value of the DSI was 1 when $P(\mathbf{Z}'_a) = 0$. This value means that the axial piston pump has entered its final failure stage at this point.

2.2.3. Degradation Status Recognition

The detailed process of the degradation status recognition of an axial piston pump has been given below:

(1) The feature vectors were extracted from the outlet pressure signals of a healthy pump, and the extracted feature vectors were used as the training samples.
(2) A GMM was constructed, the parameters of which were solved using an EM algorithm based on the training samples.
(3) Step (1) was repeated and the testing samples were obtained from the pump's discharge pressure signals that were recorded.
(4) The probability that the testing samples were generated by the constructed GMM was calculated and the DSI of the axial piston pump was ascertained based on Equation (21).

The flowchart of the proposed degradation status recognition scheme is shown in Figure 1.
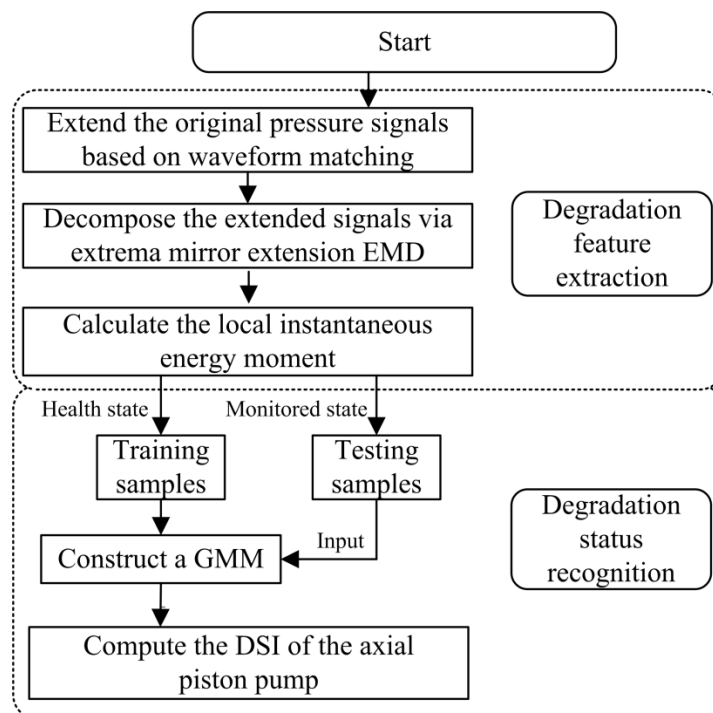

Figure 1. Overview of the degradation status identification method.

3. Validations

In order to demonstrate the effectiveness of the proposed method, two case studies are presented in this section. Given that the fault signals of many rotating machines, including axial piston pumps, exhibit quasi-periodic pulses, a simulated example is given to verify the advantage of the proposed method in dealing with the end effects when decomposing such quasi-periodic signals. In addition, the experimental signals, which were collected from the hydraulic pump test rig under different working conditions, were used to demonstrate the feasibility of the proposed degradation status identification method.

3.1. Simulation Analysis

As previously noted, the discharge pressure signals of axial piston pumps exhibit a quasi-periodic characteristic when some types of failure occur. In fact, there are many other fault signals which possess quasi-periodicity, such as vibration signals resulting from a slight looseness of a coupling, small fatigue cracks, or the rotor and stator rubbing, et al. [43,44]. In order to demonstrate the effectiveness of the proposed EMD method in processing these quasi-periodic signals, a simulated signal $p(t)$ was constructed as follows:

$$p(t) = \sin(2\pi f_1 t) + \cos(2\pi f_2 t - \pi/3) \tag{22}$$

where $f_1 = 0.25$ Hz and $f_2 = 0.5$ Hz; the sampling frequency was 10 Hz and the period was 4 s.

In order to let $p(t)$ be a quasi-periodic signal, the $p(t)$ in each period is either extracted or interpolated randomly so that the number of points in each period is between 35 and 45. It is supposed that $p^*(t)$ is the quasi-periodic signal that is obtained. The original signal of $p^*(t)$ and its ideal EMD decomposition results are shown in Figure 2.
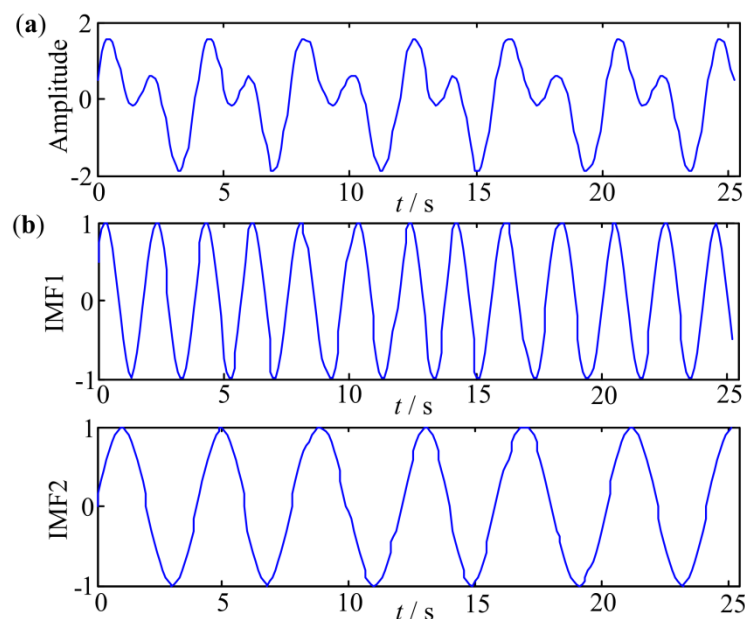

Figure 2. The signal $p^*(t)$ and its ideal empirical mode decomposition (EMD) decomposition results: (**a**) The original signal, (**b**) Two intrinsic mode functions (IMF) components.

Following this, three types of EMD algorithms were adopted to decompose the signal $p^*(t)$. Figure 3 presents the decomposition results for the three types of EMD algorithms. In Figure 3a, it can be seen that there is an obvious difference between the actual IMFs and the ideal IMFs. This shows that the results of the decomposition were significantly distorted when the EMD was used without restraining the end effects (EMD1) and the end effects greatly affected the accuracy of the decomposition. Figure 3b depicts the results of the decomposition for the EMD based on the extrema mirror extension

(EMD2). By comparing Figures 3b and 3a, it can be found that the accuracy of the IMF2 improved. This means that the EMD combining with the extrema mirror extension can restrain the end effects to some extent. However, obvious end effects still exists as the signal was intercepted in a noncomplete period in Figure 3b. Figure 3c illustrates the results of the decomposition that was obtained from the proposed EMD method (EMD3). In Figure 3c, it is clear that the deviation between the actual IMFs and the ideal IMFs was very small; this indicates that the proposed method can effectively restrain the end effects and that it obviously improved the accuracy of the decomposition.
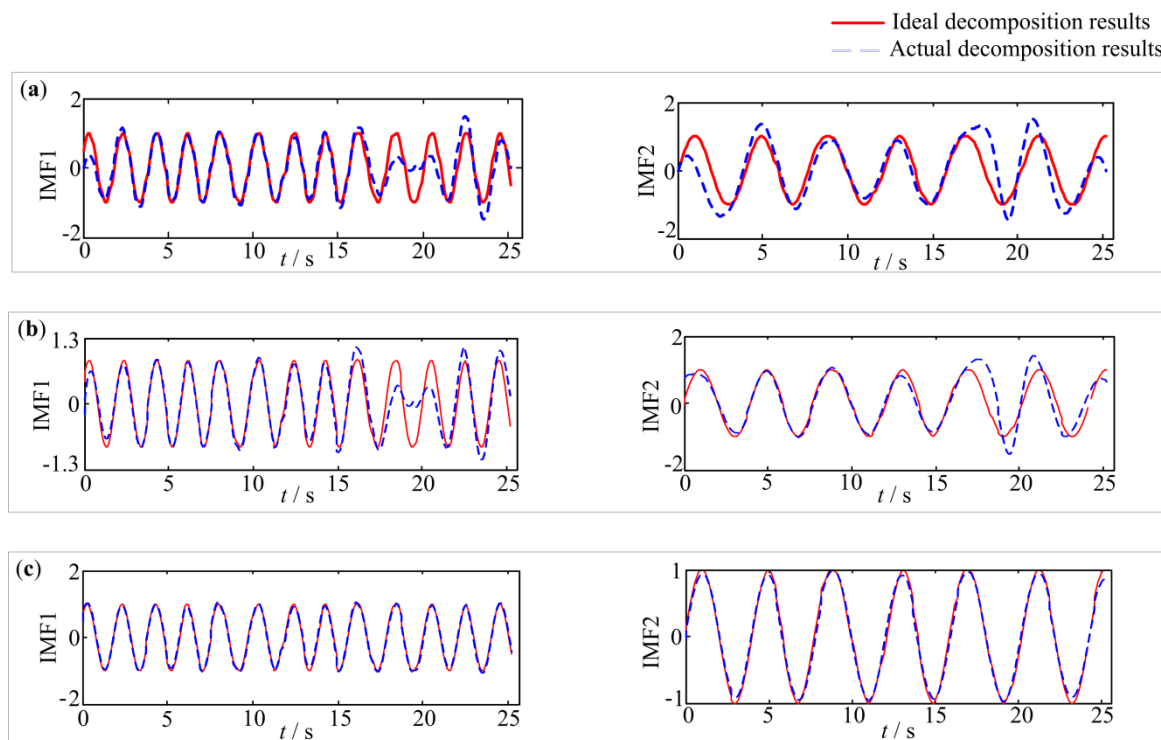
Figure 3. The decomposition results of (**a**) EMD1, (**b**) EMD2, (**c**) EMD3.

To highlight the changes from the three types of EMD methods, the Hilbert spectra of the IMFs obtained from the three types of EMD methods were then calculated, and are shown in Figure 4. In Figure 4a, it is clear that there was considerable distortion at the endpoints in the spectrum line at 0.25 Hz when using EMD1. By comparing Figure 4b with Figure 4a, the distortion at the endpoints was slightly improved; however, there was also clear distortion at the endpoints. Figure 4c shows the Hilbert spectrum of the IMFs using the proposed method. From Figure 4c, it can be observed that the spectrum line displays an almost straight line at 0.25 Hz and the spectrum line at 0.5 Hz shows only small distortion; moreover, there is almost no distortion at the endpoints. This indicates that the proposed EMD can effectively restrain the end effects and capture the IMFs with high accuracy.
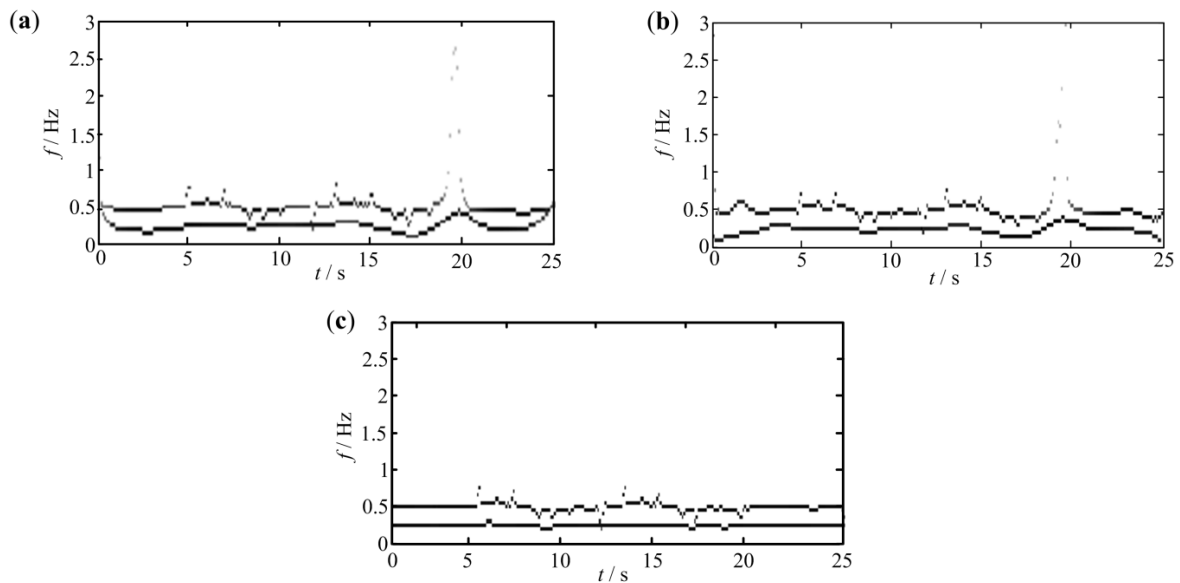
Figure 4. The Hilbert spectra of the IMFs obtained from (**a**) EMD1, (**b**) EMD2, (**c**) EMD3.

3.2. Experimental Analysis

3.2.1. Description of the Experiments

The proposed scheme was validated using an experimental platform, as shown in Figure 5. This platform chiefly consisted of an AC motor, an axial piston pump, a throttle valve, and a few hydraulic auxiliary devices. The pump that was tested had a rated speed of 1470 r/min and contained seven plungers. In this experiment, loose piston shoes with defects of different sizes were used to simulate the different degradation states of the axial piston pump. According to the technical requirements of the pump, the factory clearance between the plunger's ball head and the ball socket of the shoe is within 0.015–0.025 mm and the pump can be regarded as being in a normal state when the clearance does not exceed 0.2 mm. Therefore, four clearance values, 0.1 mm, 0.25 mm, 0.35 mm, and 0.5 mm, were chosen to simulate the normal state, slight degradation, moderate degradation, and final failure of the hydraulic pump.
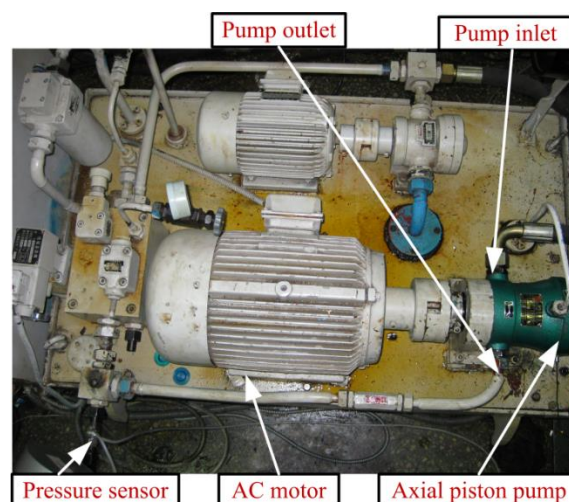

Figure 5. The experimental platform for the pump's degradation status recognition.

During the experiments, a pressure sensor, the range of which was 0–25 MPa, was used to measure the discharge pressure signals of the tested pump. With the objective of studying the applicability of

the proposed algorithm under different operating conditions, three kinds of loads were simulated by means of the throttle valve; at this point, the system's pressure was set at 8 MPa, 10 MPa, and 15 MPa. Twelve groups of experiments were conducted on this platform. The data acquisition system was composed of an industrial computer and a National Instrument (NI, Austin, TX, USA) USB-6221 board. The data acquisition software was developed using NI LabVIEW® 8.6. The data sampling rate was 2 kHz, and each set of data collection lasted for 10 s for each clearance at the same pressure; consequently, 12 groups of pressure signals were collected. The data obtained for a pressure of 10 MPa and a clearance of 0.1 mm were used for training and the remaining 11 data sets were used for testing.

3.2.2. Degradation Status Recognition of Axial Piston Pumps

As described in Section 2, the features that can characterize the degradation states of an axial piston pump under variable operating conditions must first be extracted. To summarize the paper, the data from the normal and slight degradation states were analyzed to explain the process of feature extraction. Figure 6 illustrates the time-domain waveforms and the power spectra of the discharge pressure signals from the two states, i.e., normal and slight degradation.
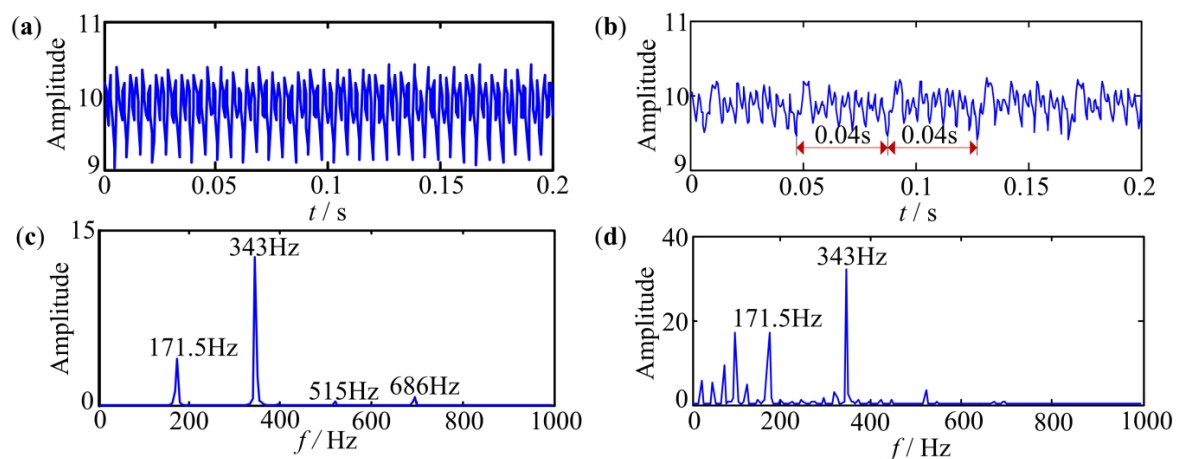

Figure 6. The original signals from (**a**) a normal pump and (**b**) a pump with slight degradation, and the power spectra of the signals from (**c**) a normal pump and (**d**) a pump with slight degradation.

From Figure 6, it can be seen that the outlet pressure signals of the two states were quasi-periodic. Meanwhile, it can also be seen that the pulsation periods of the pressure signals of the two states were 0.0058 s and 0.04 s, which was consistent with the failure mechanism analysis of axial piston pumps. Subsequently, the original pressure signals were decomposed by EMD2 and EMD3; the results of the decomposition are illustrated in Figure 7. Figure 7a,b shows the IMFs that were obtained from the two types of EMD methods from the normal pump's outlet pressure signal. By comparing Figures 7a and 7b, it can be observed that there was little difference between the first three IMF components IMF1–IMF3 of the two methods. Nevertheless, it is obvious that the fifth IMF component IMF5 of the two methods had a big effect. A possible reason for this is that the influence of the end effects is small in IMF components with a high frequency, but the decomposition errors that originated from the end effects will gradually accumulate in the IMF components with a low frequency as the sifting process is carried out; similar results can also be found in Figure 7c,d. In order to further describe this difference, Figure 8 depicts the Hilbert spectra of IMF5 obtained from the two methods.
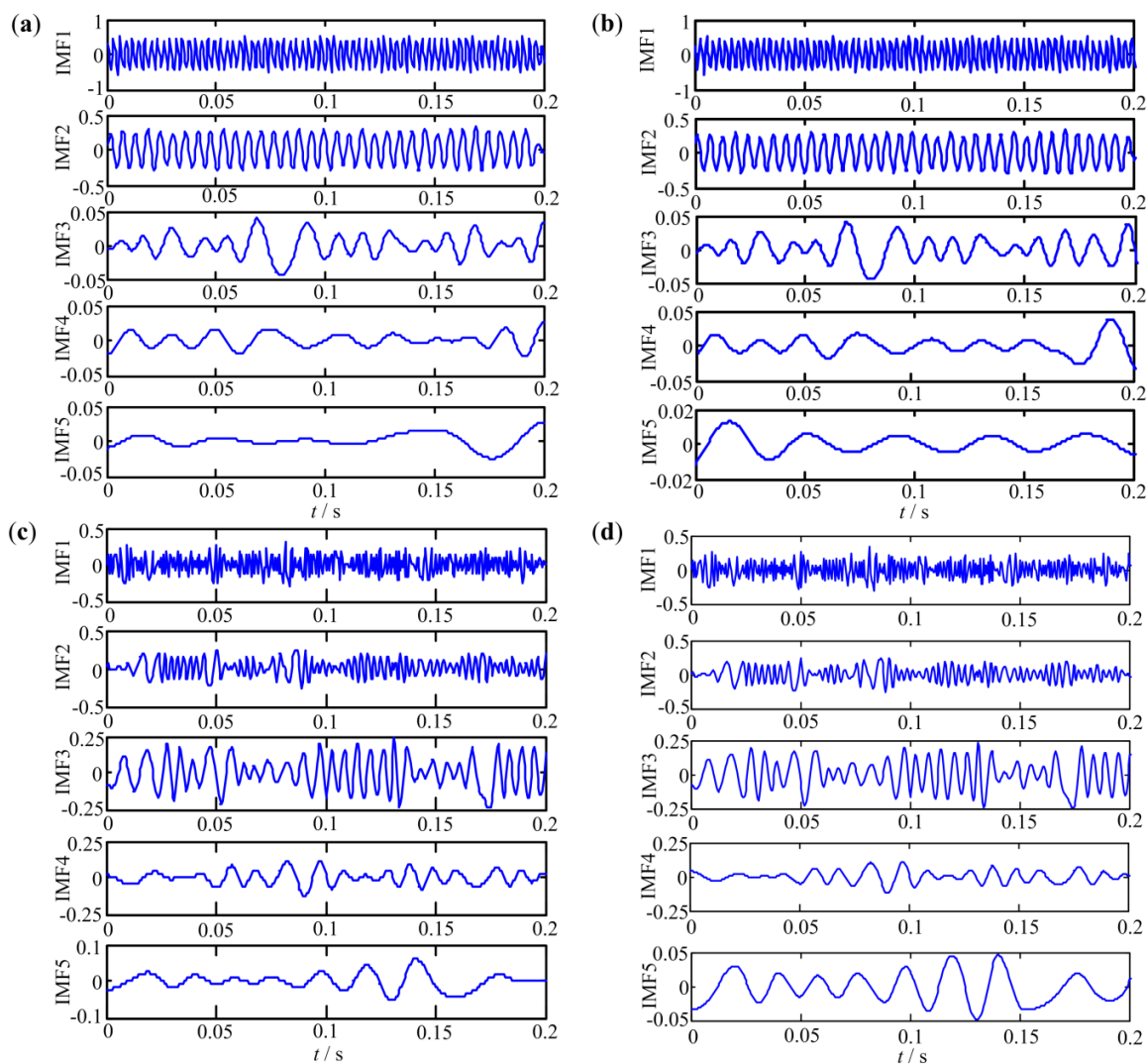
Figure 7. The decomposition results for the normal pressure signals using (**a**) EMD2, (**b**) EMD3, and the results for the slight degradation pressure signals using (**c**) EMD2, (**d**) EMD3.

From Figure 8a,c, it can be found that the two spectrum lines show significant divergence at the endpoints, which the arrows point to. This indicates that distinct end effects occur when EMD2 is used. Compared with Figure 8a,c, it can be seen that the distortion at the endpoints shown in Figure 8b,d significantly improved. In particular, the spectrum line shown in Figure 8d is almost a straight line. This proves that the proposed EMD can effectively restrain the end effects.

After more accurate IMF components are obtained, based on the proposed EMD, the local instantaneous energy moment entropy could be computed from Equation (18). For each set of data, a 0.2 s signal segment was extracted to calculate the feature entropy and this process was repeated 25 times. Therefore, there are 25 feature entropies for each set of data and the number of total feature entropies is 300 for the 12 sets of data. Figure 9 shows the obtained feature entropies.

It can be seen from Figure 9 that the feature entropy values of the different degradation states are obviously different and the values of the feature entropies increased as the degree of degradation increased. Meanwhile, for the same degree of degradation, even if the system operating conditions were different, the fluctuation in the feature entropy values was small. This means that the proposed feature entropy can not only effectively characterize the degree of degradation of axial piston pumps but it can also be applied for variable operating conditions.
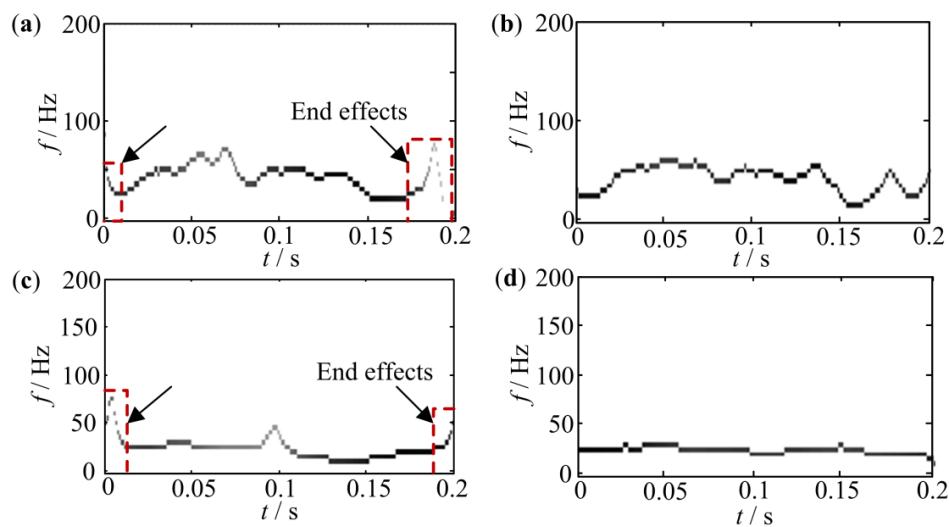
Figure 8. The Hilbert spectrum for the IMF5 of the normal pressure signals using (**a**) EMD2 and (**b**) EMD3, and the Hilbert spectrum for the slight degradation pressure signals using (**c**) EMD2 and (**d**) EMD3.
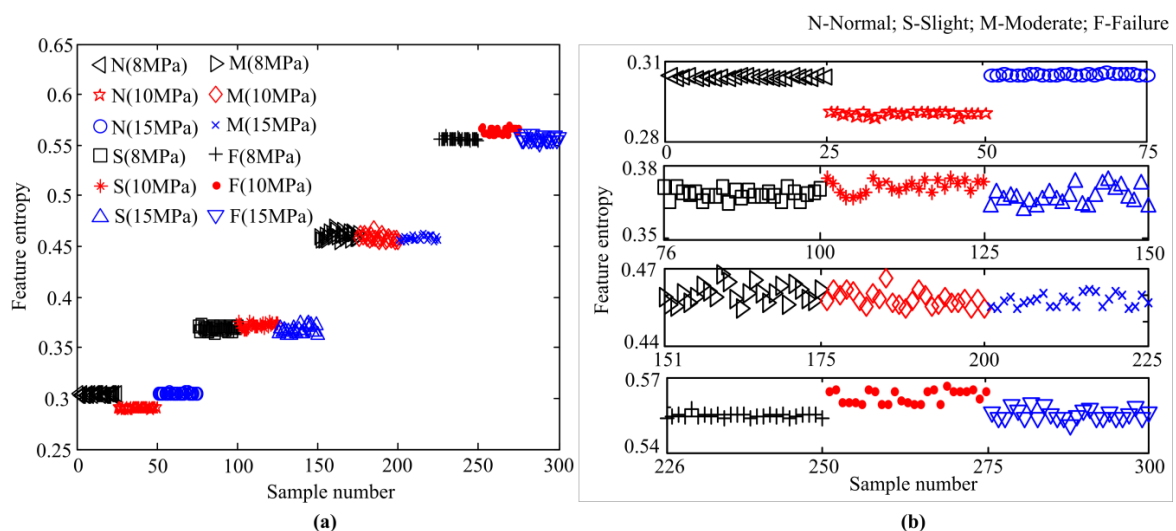

Figure 9. The local instantaneous energy moment entropy obtained from EMD3 under different working conditions: (**a**) All samples and (**b**) partially enlarged drawings.

In contrast, the feature entropy, based on the EMD2 method, was also calculated and the calculation results are shown in Figure 10. From Figure 10, one can see that the obtained feature entropy, based on EMD2, was also able to effectively characterize the degree of deterioration of the axial piston pump. These results prove the feasibility of the method of degradation feature extraction based on EMD that was proposed in this paper. By comparing Figures 9 and 10, although the difference in the feature entropies obtained from two EMD methods was small under normal conditions, the fluctuation of the feature entropies of the remaining three states was significantly greater than that shown in Figure 9. A possible reason for this is that the low-frequency component energy moment under normal conditions was small, but the low-frequency component's energy moment gradually increased as the degree of degradation increased. At this point, the accuracy of the low-frequency component had a greater influence on the entropy values than that of the high-frequency component.
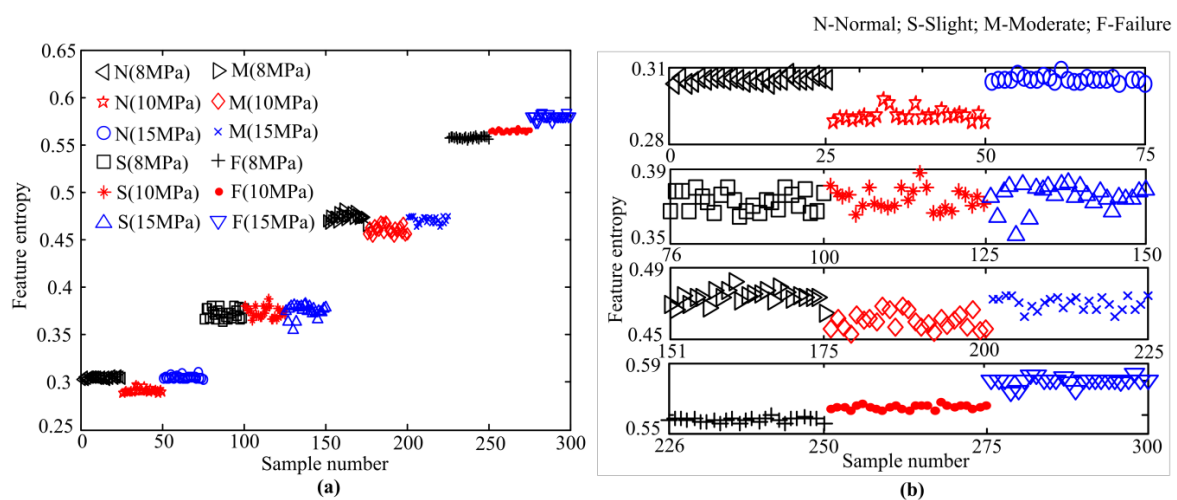
Figure 10. The feature entropy obtained from EMD2 for the different working conditions: (**a**) All samples and (**b**) partially enlarged drawings.

After the feature entropies of the different states of the axial piston pumps were obtained, the feature entropies of the normal state were chosen to construct the GMM. Subsequently, all of the feature entropies were inputted into the constructed GMM to count the DSI, according to Equation (21). Figure 11 depicts the DSI sequences obtained from the GMM using the two EMD methods.
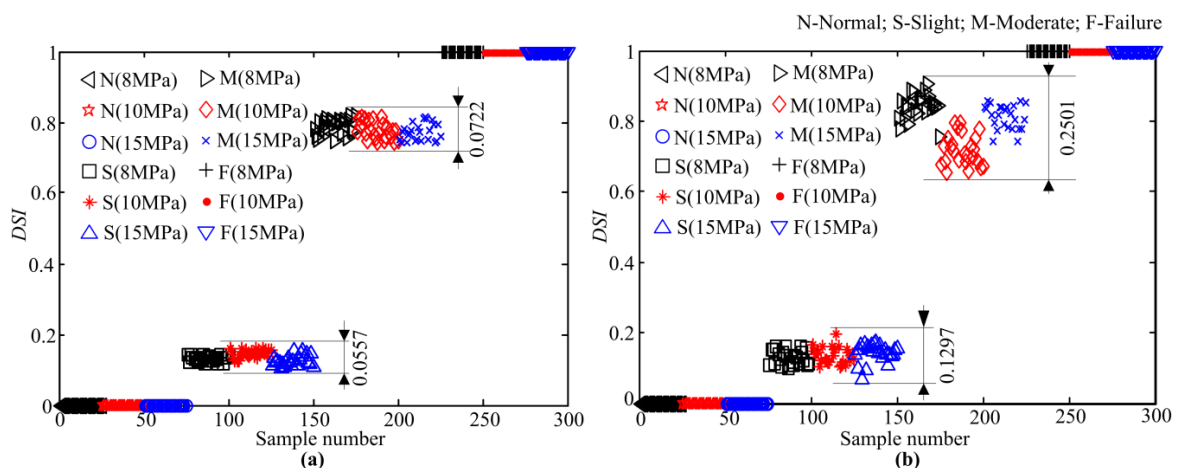

Figure 11. The degradation status index (DSI) sequences obtained from the Gaussian mixture model (GMM) using (**a**) EMD3 and (**b**) EMD2.

As shown in Figure 11a, the DSI based on the proposed method was able to accurately distinguish four states of the axial piston pumps. Meanwhile, the overall trend of the DSI kept increasing with the increase of the degree of degradation, and the DSI did not fluctuate much for the same degree of degradation; this means that a reasonable threshold can be set to effectively recognize the degradation state of the pumps in practical applications. Compared with Figure 11a, the four statuses of the axial piston pumps can also be identified in Figure 11b, but the DSI values shown in Figure 11b fluctuated violently; this was especially the case where the fluctuating value reached 0.2501 when the pump was in the moderate degradation stage, and this greatly reduced the accuracy of the degradation status recognition.

3.2.3. Further Comparison and Discussion

In order to further verify the proposed method, a few comparisons were conducted from two viewpoints. On the one hand, a few of the indicators presented in previous publications were compared to prove the advantage of the proposed feature entropy method when characterizing the degree of degradation of a pump under variable operating conditions. On the other hand, some modeling methods, including SOM, FCM, and SVDD, were also selected for a comparison.

Time-domain indicators, such as the root mean square (RMS), the waveform index (WI), the skewness index (SI), and the kurtosis index (KI), have been widely used for degradation feature extraction when identifying the degradation states of rotating machines. Figure 12 shows the extracted time-domain indices of the different states under a pressure of 10 MPa. As illustrated in Figure 12a, the RMS values of the normal state and the degradation states were obviously different, but those of the three degradation states were almost the same, around 0.035. Unlike the RMS indicator, Figure 12b–d illustrates the values of the other three dimensionless time-domain indices for the different states. Although the difference in each indicator value became larger under the different degradation states, it was still difficult to effectively distinguish between the three degradation states. This indicates that it was difficult to use the traditional time-domain indicators to effectively monitor the degradation trend of axial piston pumps.
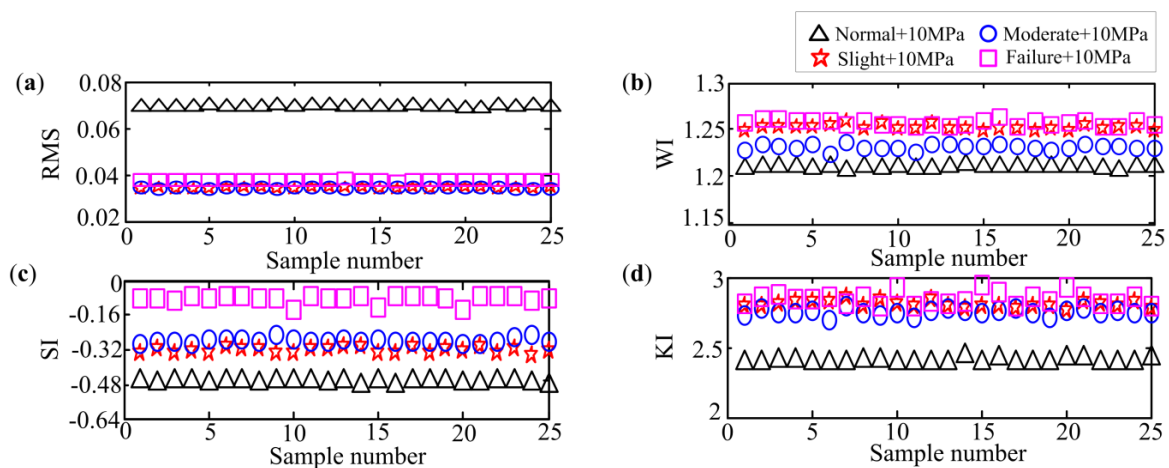

Figure 12. The commonly used time-domain degradation indices. (**a**) Root mean square (RMS); (**b**) waveform index (WI); (**c**) skewness index (SI); (**d**) kurtosis index (KI).

Based on the previous analysis, it is clear that the energy distribution of the signal will change when the pump's state changes. Considering that the information entropy is able to describe the distribution characteristic of the signal, some of the information entropies, including power spectrum Shannon entropy (PSE1), power spectrum exponential entropy (PSE2), singular spectrum Shannon entropy (SSE1), singular spectrum exponential entropy (SSE2), SE and permutation entropy (PE) [45], which have been applied in the field of degradation recognition, were used to characterize the degradation states of the pump. The calculated information entropies are depicted in Figure 13.

From Figure 13a,b, it can be seen that the entropies that were based on the power spectrum could not distinguish between the four states; a possible reason for this is that power spectrum analysis is a global transform. As shown in Figure 13c,d, the effect of the singular spectrum entropies was better than that of the power spectrum entropies, but the trend of the singular spectrum entropies was not monotonous as the degree of degradation increased. This means that it was difficult to use them to track the degradation trend of the pump. From Figure 13e,f, similar conclusions could be drawn, this is because these two kinds of entropies, shown in Figure 13e,f, were calculated in the original time-domain space, which means that the calculation results were easily disturbed by the noise.
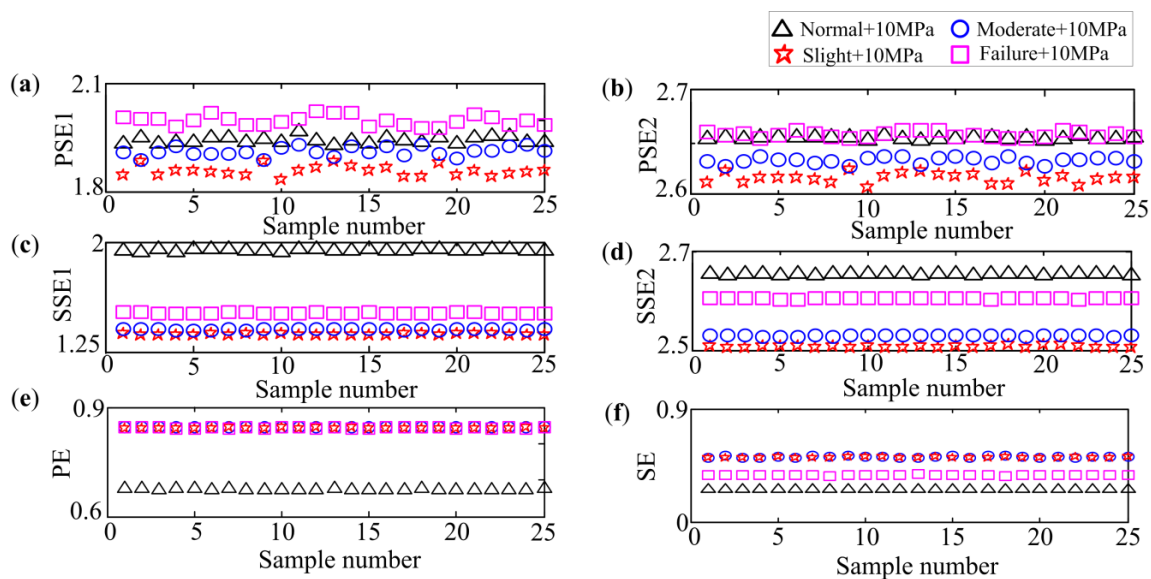
Figure 13. Six kinds of information entropies. (**a**) Power spectrum Shannon entropy (PSE1); (**b**) power spectrum exponential entropy (PSE2); (**c**) singular spectrum Shannon entropy (SSE1); (**d**) singular spectrum exponential entropy (SSE2); (**e**) permutation entropy (PE); (**f**) sample entropy (SE).

After carrying out the comparisons of the degradation indicators, the deterioration recognition methods were compared with the proposed GMM method. As previously noted, although many of the recognition methods have shown remarkable capability, most of these methods require samples of different degradation states to train the recognition model. However, it is not the case that the degradation process of a pump is always the same. This means that it was difficult to obtain standard training samples for all of the degradation states. Unlike these methods, the SOM-based method and SVDD-based method only require samples of the normal state, and the FCM-based method only needs normal samples and a final failure sample for the model to work. Hence, these three methods are compared in this paper. Figure 14 shows the recognition results based on SOM.
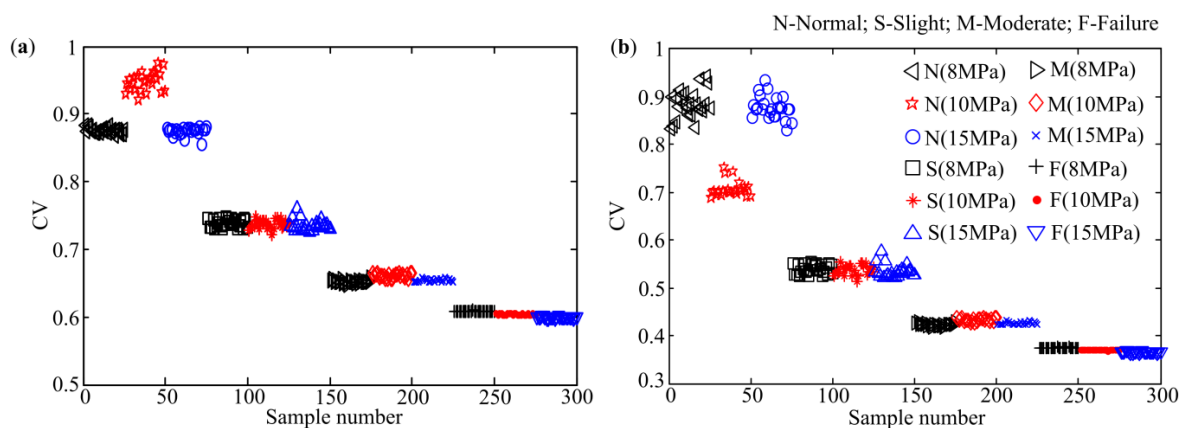

Figure 14. The self-organization mapping (SOM)-based recognition results for the different SOM parameters. (**a**) Scale parameter selects 0.5 and (**b**) scale parameter selects 0.2.

As can be seen in Figure 14, the degradation process of the pump can be divided into four stages. However, it is obvious that the identification results were different when selecting the different SOM parameters; this will seriously affect the applicability of the SOM method. Figure 15 presents the recognition results using the SVDD and FCM methods.
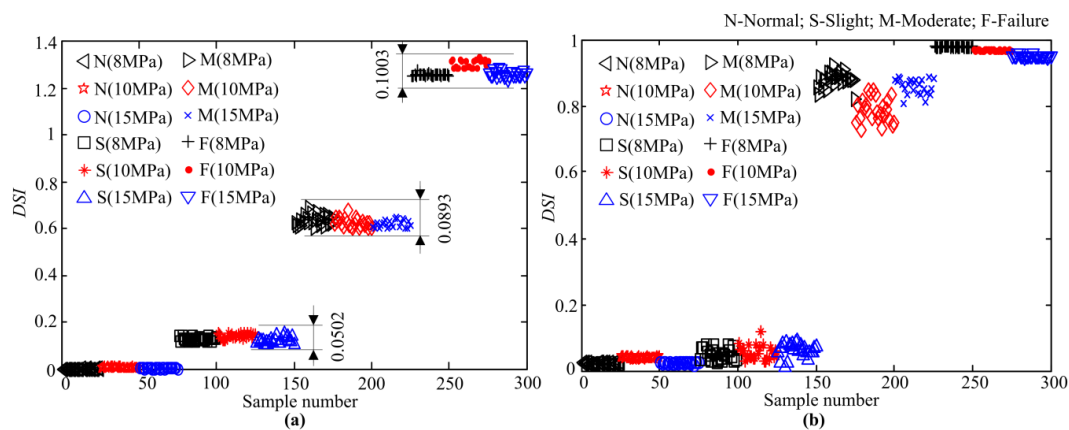
Figure 15. The recognition results based on (**a**) support vector data description (SVDD) and (**b**) fuzzy c-means clustering (FCM).

From Figure 15a, it can be observed that the four states of the pump can be clearly distinguished and the fluctuation of the DSI of the same fault size was small under variable operating conditions. Comparing Figure 15b with Figure 15a, we find that it is difficult to distinguish some samples of the normal state and the slight degradation state when using FCM method. Meanwhile, the DSI values obtained for the moderate degradation state fluctuated violently. This means that the SVDD method is better than FCM method when performing the degradation states' recognition of the pump. Nevertheless, the results shown in Figure 15a fluctuate more violently than those shown in Figure 11a, which proves that the proposed method can identify the degradation states of the pump with higher accuracy.

4. Conclusions

In this paper, a new approach to identify the degradation status of axial piston pumps has been presented. Unlike the traditional method that concentrates on recognizing different failure types or fault sizes under constant operating conditions, this study mainly focused on identifying methods that can reliably track the degradation status of a pump under variable conditions. Based on the aforementioned illustration, the presented scheme included improved EMD-based feature extraction and GMM-based degradation status recognition. According to both the simulation and experimental results, the following conclusions could be drawn:

(1) The proposed method can effectively restrain the end effects of the EMD and more accurately capture the IMF components when processing periodic signals or quasi-periodic signals.

(2) The local instantaneous energy moment entropy is able to successfully characterize the degree of degradation of a pump under variable conditions and is better than traditional indicators, such as the RMS, the kurtosis index, PSE, or SSE.

(3) The DSI that was derived from the GMM is able to identify and track the current deterioration stage of a pump, thus enabling the realization of fault prognostics.

Further research will explore how better to restrain the end effects of EMD when decomposing irregular or strongly stochastic signals. In addition, degradation states' recognition under multi-faults will be paid more attention in future research.

Author Contributions: Conceptualization, C.L. and S.W.; Methodology, C.L.; Writing—Original Draft Preparation, C.L.; Writing—Review & Editing, C.L.; Software and data collection; Z.Z.; Supervision, S.W. All authors have read and agreed to the published version of the manuscript.

Conflicts of Interest: The authors declare no conflict of interest.

References

1. Liu, H.; Zhang, J.; Lu, C. Performance degradation prediction for a hydraulic servo system based on Elman network observer and GMM–SVR. *Appl. Math. Model.* **2015**, *39*, 5882–5895. [CrossRef]
2. Wang, X.; Lin, S.; Wang, S.; He, Z.; Zhang, C. Remaining useful life prediction based on the Wiener process for an aviation axial piston pump. *Chin. J. Aeronaut.* **2016**, *29*, 779–788. [CrossRef]
3. Ma, Z.; Wang, S.; Shi, J.; Li, T.; Wang, X. Fault diagnosis of an intelligent hydraulic pump based on a nonlinear unknown input observer. *Chin. J. Aeronaut.* **2018**, *31*, 385–394. [CrossRef]
4. Guo, R.; Zhao, Z.; Huo, S.; Jin, Z.; Zhao, J.; Gao, D. Research on State Recognition and Failure Prediction of Axial Piston Pump Based on Performance Degradation Data. *Processes* **2020**, *8*, 609. [CrossRef]
5. Wang, Y.-K.; Li, H.-R.; Wang, B.; Xu, B.-H. Spatial Information Entropy and Its Application in the Degradation State Identification of Hydraulic Pump. *Math. Probl. Eng.* **2015**, *2015*, 1–11. [CrossRef]
6. Li, H.; Sun, J.; Ma, H.; Tian, Z.; Li, Y. A novel method based upon modified composite spectrum and relative entropy for degradation feature extraction of hydraulic pump. *Mech. Syst. Signal Process.* **2019**, *114*, 399–412. [CrossRef]
7. Hancock, K.M.; Zhang, Q. Maintenance and Fault Diagnosis Tools for Hydraulic Pumps. In Proceedings of the 50th National Conference on Fluid Power, Las Vegas, NV, USA, 16–18 March 2005; pp. 363–369.
8. Gao, Y.; Zhang, Q. A Wavelet Packet and Residual Analysis Based Method for Hydraulic Pump Health Diagnosis. *Proc. Inst. Mech. Eng. Part D J. Automob. Eng.* **2006**, *220*, 735–745. [CrossRef]
9. Zhao, Z.; Jia, M.; Wang, F.; Wang, S. Intermittent chaos and sliding window symbol sequence statistics-based early fault diagnosis for hydraulic pump on hydraulic tube tester. *Mech. Syst. Signal Process.* **2009**, *23*, 1573–1585. [CrossRef]
10. Lu, C.; Wang, S.; Makis, V. Fault severity recognition of aviation piston pump based on feature extraction of EEMD paving and optimized support vector regression model. *Aerosp. Sci. Technol.* **2017**, *67*, 105–117. [CrossRef]
11. Lei, Y.; He, Z.; Zi, Y. Application of an intelligent classification method to mechanical fault diagnosis. *Expert Syst. Appl.* **2009**, *36*, 9941–9948. [CrossRef]
12. Dou, D.; Zhou, S. Comparison of four direct classification methods for intelligent fault diagnosis of rotating machinery. *Appl. Soft Comput.* **2016**, *46*, 459–468. [CrossRef]
13. Zheng, Z.; Xin, G. Fault Feature Extraction of Hydraulic Pumps Based on Symplectic Geometry Mode Decomposition and Power Spectral Entropy. *Entropy* **2019**, *21*, 476. [CrossRef]
14. Caraiani, P. The predictive power of singular value decomposition entropy for stock market dynamics. *Phys. A Stat. Mech. Appl.* **2014**, *393*, 571–578. [CrossRef]
15. Delgado-Bonal, A.; Marshak, A. Approximate Entropy and Sample Entropy: A Comprehensive Tutorial. *Entropy* **2019**, *21*, 541. [CrossRef]
16. Cui, H.; Zhang, L.; Kang, R.; Lan, X. Research on fault diagnosis for reciprocating compressor valve using information entropy and SVM method. *J. Loss Prev. Process. Ind.* **2009**, *22*, 864–867. [CrossRef]
17. Fei, C.; Bai, G.-C.; Tang, W.; Ma, S. Quantitative Diagnosis of Rotor Vibration Fault Using Process Power Spectrum Entropy and Support Vector Machine Method. *Shock. Vib.* **2014**, *2014*, 1–9. [CrossRef]
18. Hu, G.; Zhu, F.; Ren, Z. Power quality disturbance identification using wavelet packet energy entropy and weighted support vector machines. *Expert Syst. Appl.* **2008**, *35*, 143–149. [CrossRef]
19. Lu, C.; Wang, S.; Tomovic, M. Fault severity recognition of hydraulic piston pumps based on EMD and feature energy entropy. In Proceedings of the 2015 IEEE 10th Conference on Industrial Electronics and Applications (ICIEA), Auckland, New Zealand, 15–17 June 2015; pp. 489–494.
20. Moreno-Gomez, A.; Amezquita-Sanchez, J.; Valtierra-Rodriguez, M.; Perez-Ramirez, C.A.; Dominguez-Gonzalez, A.; Chavez-Alegria, O. EMD-Shannon Entropy-Based Methodology to Detect Incipient Damages in a Truss Structure. *Appl. Sci.* **2018**, *8*, 2068. [CrossRef]
21. Bafroui, H.H.; Ohadi, A.R. Application of wavelet energy and Shannon entropy for feature extraction in gearbox fault detection under varying speed conditions. *Neurocomputing* **2014**, *133*, 437–445. [CrossRef]
22. Liu, C.; Zhu, L.; Ni, C. Chatter detection in milling process based on VMD and energy entropy. *Mech. Syst. Signal Process.* **2018**, *105*, 169–182. [CrossRef]

23. He, Z.; Shen, Y.; Wang, Q.; Wang, Y.; Feng, N.; Ma, L. Mitigating end effects of EMD using non-equidistance grey model. *J. Syst. Eng. Electron.* **2012**, *23*, 603–611. [CrossRef]

24. Lin, D.-C.; Guo, Z.-L.; An, F.-P.; Zeng, F.-L. Elimination of end effects in empirical mode decomposition by mirror image coupled with support vector regression. *Mech. Syst. Signal Process.* **2012**, *31*, 13–28. [CrossRef]

25. Liu, X.; Bo, L.; Luo, H. Bearing faults diagnostics based on hybrid LS-SVM and EMD method. *Measurement* **2015**, *59*, 145–166. [CrossRef]

26. Chu, P.C.; Fan, C.; Huang, N. Derivative-optimized empirical mode decomposition for the Hilbert–Huang transform. *J. Comput. Appl. Math.* **2014**, *259*, 57–64. [CrossRef]

27. Yan, J.; Lu, L. Improved Hilbert–Huang transform based weak signal detection methodology and its application on incipient fault diagnosis and ECG signal analysis. *Signal Process.* **2014**, *98*, 74–87. [CrossRef]

28. Wang, J.; Liu, W.; Zhang, S. An approach to eliminating end effects of EMD through mirror extension coupled with support vector machine method. *Pers. Ubiquitous Comput.* **2019**, *23*, 443–452. [CrossRef]

29. Rilling, G.; Flandrin, P.; Goncalves, P. On empirical mode decomposition and its algorithms. In Proceedings of the IEEE-EURASIP Workshop on Nonlinear Signal and Image Processing, Grado, Italy, 8–11 June 2003; Volume 3, pp. 8–11.

30. Lu, C.; Wang, S.; Zhang, C. Fault diagnosis of hydraulic piston pumps based on a two-step EMD method and fuzzy C-means clustering. *Proc. Inst. Mech. Eng. Part C J. Mech. Eng. Sci.* **2016**, *230*, 2913–2928. [CrossRef]

31. Zhang, X.; Liang, Y.; Zhou, J.; Zang, Y. A novel bearing fault diagnosis model integrated permutation entropy, ensemble empirical mode decomposition and optimized SVM. *Measurement* **2015**, *69*, 164–179. [CrossRef]

32. Duan, L.X.; Xie, M.Y.; Bai, T.B.; Wang, J. A new support vector data description method for machinery fault diagnosis with unbalanced datasets. *Expert Syst. Appl.* **2016**, *64*, 239–246. [CrossRef]

33. Soualhi, A.; Medjaher, K.; Zerhouni, N. Bearing Health Monitoring Based on Hilbert–Huang Transform, Support Vector Machine, and Regression. *IEEE Trans. Instrum. Meas.* **2014**, *64*, 52–62. [CrossRef]

34. Zhang, B.; Zhang, S.; Li, W. Bearing performance degradation assessment using long short-term memory recurrent network. *Comput. Ind.* **2019**, *106*, 14–29. [CrossRef]

35. Hong, S.; Zhou, Z.; Zio, E.; Hong, K. Condition assessment for the performance degradation of bearing based on a combinatorial feature extraction method. *Digit. Signal Process.* **2014**, *27*, 159–166. [CrossRef]

36. Zhang, Y.; Tang, B.; Han, Y.; Deng, L. Bearing performance degradation assessment based on time-frequency code features and SOM network. *Meas. Sci. Technol.* **2017**, *28*, 045601. [CrossRef]

37. Tong, Q.J.; Hu, J.Z. Bearing performance degradation assessment based on information-theoretic metric learning and fuzzy C-means clustering. *Meas. Sci. Technol.* **2020**, *31*, 075001.

38. Wang, B.; Hu, X.; Li, H. Rolling bearing performance degradation condition recognition based on mathematical morphological fractal dimension and fuzzy C-means. *Measurement* **2017**, *109*, 1–8. [CrossRef]

39. Pan, Y.; Chen, J.; Li, X. Bearing performance degradation assessment based on lifting wavelet packet decomposition and fuzzy c-means. *Mech. Syst. Signal Process.* **2010**, *24*, 559–566. [CrossRef]

40. Bin, G.; Gao, J.; Li, X.; Dhillon, B. Early fault diagnosis of rotating machinery based on wavelet packets—Empirical mode decomposition feature extraction and neural network. *Mech. Syst. Signal Process.* **2012**, *27*, 696–711. [CrossRef]

41. Lei, Y.; Lin, J.; He, Z.; Zuo, M.J.; Zuo, M.J. A review on empirical mode decomposition in fault diagnosis of rotating machinery. *Mech. Syst. Signal Process.* **2013**, *35*, 108–126. [CrossRef]

42. Dempster, A.P.; Laird, N.M.; Rubin, D.B. Maximum Likelihood from Incomplete Data Via theEMAlgorithm. *J. R. Stat. Soc. Ser. B Methodol.* **1977**, *39*, 1–22. [CrossRef]

43. Inoue, T.; Sueoka, A.; Kanemoto, H.; Odahara, S.; Murakami, Y. Detection of minute signs of a small fault in a periodic or a quasi-periodic signal by the harmonic wavelet transform. *Mech. Syst. Signal Process.* **2007**, *21*, 2041–2055. [CrossRef]

44. Peng, Z.; Chu, F.; Tse, P.W. Detection of the rubbing-caused impacts for rotor–stator fault diagnosis using reassigned scalogram. *Mech. Syst. Signal Process.* **2005**, *19*, 391–409. [CrossRef]

45. Unakafova, V.; Keller, K. Efficiently Measuring Complexity on the Basis of Real-World Data. *Entropy* **2013**, *15*, 4392–4415. [CrossRef]